Phase Evolution During Heat Treatment of Nb_3Sn Wires Under Development for the FCC Study

Simon C. Hopkins, Algirdas Baskys, Amalia Ballarino, Jonas Lachmann, and Andreas Leineweber

***Abstract*—In recent years, the phase formation sequence during heat treatment of Nb_3Sn wires, and the influence of the microstructure and compositional homogeneity of Nb_3Sn on in-field critical current (I_c), have received increasing attention. For RRP wires, the importance of understanding and managing the formation of the ternary phase nausite has been demonstrated. However, a published Cu–Nb–Sn phase diagram including this phase is still not available; and conductor development for the Future Circular Collider (FCC) study has introduced a variety of less-studied internal tin wire layouts. In this article, a study of phase transformations in the ternary Cu–Nb–Sn system is summarized, and selected isothermal sections of the re-evaluated phase diagram are presented. The phase transformations during low-temperature heat treatment steps of wires developed for the FCC study are also presented and analyzed in comparison to established RRP conductors.**

***Index Terms*—Heat treatment, Intermetallic, Microstructure, Multifilamentary superconductors, Niobium-tin.**

I. Introduction

THE development of Nb_3Sn accelerator magnets for the High Luminosity LHC (HL-LHC) Project at CERN, and proposals for high-field Nb_3Sn magnets for an energy-frontier Future Circular Collider (FCC), have led to a resurgence of research activity in Nb_3Sn superconducting wires in recent years. For FCC, challenging performance targets have been set, notably a non-copper critical current density (J_c) of 1500 A mm^{-2} at 16 T and 4.2 K, and an effective filament diameter (d_{eff}) of 20 μm [1].

An important recent contribution was the reassessment of heat treatment design for Restacked Rod Process (RRP) wires (Bruker OST) undertaken by Sanabria *et al.* [2], [3]. Conventional heat treatments include steps at around 210 °C and 400 °C, followed by the reaction step that forms Nb_3Sn at 650–665 °C (Fig. 1), but the low temperature steps were not well understood. Sanabria *et al.* were able to demonstrate the importance of controlling nausite formation, and that a heat treatment step at ~370 °C could increase J_c, avoiding the reduction often found in wires with small sub-elements [2], [3].

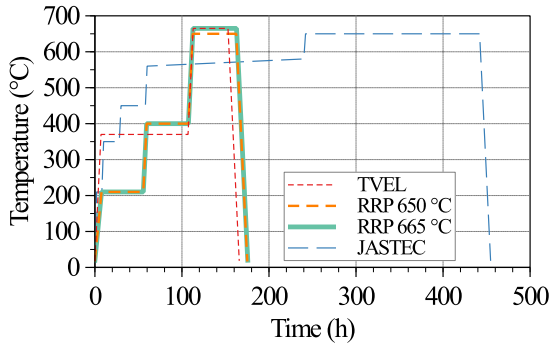

Fig. 1. Heat treatment cycles used at CERN for reacting wires of the type in Table I, based on manufacturer recommendations.

Nausite is a Sn-rich Cu–Nb–Sn phase, which was first identified surprisingly recently. The phase is named after M. Naus, who reported it in 2002 [4], but its structure and nominal composition $(Nb_{0.75}Cu_{0.25})Sn_2$ were not reported until 2017 [5], and it does not appear in published phase diagrams [6].

Sanabria's study of RRP wires confirmed that during a 215 °C step, outward diffusion of Sn from the Sn core into the surrounding Cu results in the formation of successive Cu–Sn phases in the sequence η (Cu_6Sn_5), ε (Cu_3Sn) and α Cu(Sn) as expected; sometimes with a localized region of a high-tin phase penetrating a few layers into the Nb filament region. The inclusion or omission of this step had no impact on the microstructure after the 400 °C step. During the 400 °C step, a nausite 'membrane' forms at the interface between the core and the Nb filament region, which progressively thickens, retaining Sn in the core but permitting the inward diffusion of Cu, resulting in a decreasing η content in the core [2], [3].

In addition to this influence on Cu and Sn interdiffusion, the significance of nausite is that it consumes both Nb and Sn, and it is believed to subsequently decompose to coarse and/or disconnected Nb_3Sn, thereby reducing the volume fraction of fine-grained current-carrying Nb_3Sn. The 'nausite control' heat treatments proposed by Sanabria *et al.* had the goal of minimizing the volume of nausite formed while maximizing inward Cu diffusion, and hence the conversion of η to ε in the core below the decomposition of η at 408 °C [2], [3].

In the context of its FCC conductor development program, CERN is undertaking collaborative projects with wire manufacturers to develop Nb_3Sn wires towards FCC performance requirements [7]. This has resulted in new variants of distributed barrier and distributed tin wires, which have not

Manuscript received December 1, 2020; revised January 31, 2021; accepted February 12, 2021. Date of publication March 3, 2021; date of current version June 24, 2021. The work at TU Bergakademie Freiberg was supported by CERN under collaboration Agreement KE3985. *(Corresponding author: Simon C. Hopkins.)*

Simon C. Hopkins, Algirdas Baskys, and Amalia Ballarino are with the European Organization for Nuclear Research (CERN), 1211 Geneva, Switzerland (e-mail: simon.hopkins@cern.ch; algirdas.baskys@cern.ch; amalia.ballarino@cern.ch).

Jonas Lachmann and Andreas Leineweber are with the Institute of Materials Science, TU Bergakademie Freiberg, 09599 Freiberg, Germany (e-mail: jonas.lachmann@iww.tu-freiberg.de; andreas.leineweber@iww.tu-freiberg.de).

Color versions of one or more figures in this article are available at https://doi.org/10.1109/TASC.2021.3063675.

Digital Object Identifier 10.1109/TASC.2021.3063675

TABLE I
WIRE SAMPLES

Category	Manufacturer	Wire diameter (mm)	Layout[a]	Sub-element size (μm)[b]	Nb:Sn ratio[c]
Distributed barrier	TVEL	1.0	120/127	60	-
	Bruker	1.0	162/169	58	3.4
	OST	0.85	108/127	54	3.6
	(RRP®)	0.7	78/91	54	
Distributed tin	JASTEC	0.8	139/211	32	-

[a]Layout *A*/*B*. For distributed barrier, A = superconducting sub-elements and B = total stacked units (the balance being Cu). For distributed tin, A = multi-filamentary Nb modules and B = total modules (the balance being Sn).
[b]For distributed barrier wires, the nominal diameter of the sub-element; for the distributed tin wire, the nominal diameter of the module of Nb filaments.
[c]The sub-element Nb:Sn stoichiometry, if known. All wires are Ti-doped.

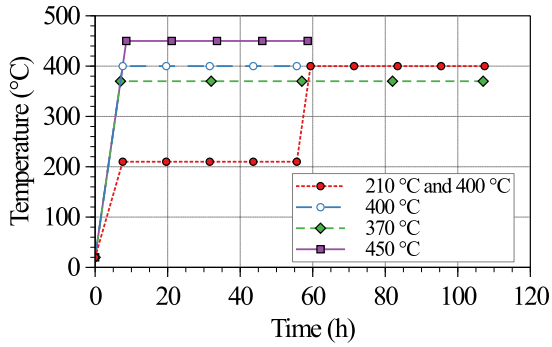

Fig. 2. Heat treatments used in this study: points mark the steps at which samples were removed from the furnace and quenched to room temperature.

been as extensively characterized as RRP wires. In parallel, a collaborative project with TU Bergakademie Freiberg is seeking to better understand the Cu–Nb–Sn system and its interactions with dopants, alloying elements and internal oxidation designs. A detailed study of the relationship between $NbSn_2$ and nausite has recently been published [8], and a re-evaluation of the Cu–Nb–Sn phase diagram is in preparation. In this article, initial findings of this study are reported, including the stability range of nausite and isothermal sections of the ternary phase diagram. The phase transformations during the low-temperature heat treatment steps of recent distributed tin and distributed barrier designs are then analyzed and compared to RRP wires procured for CERN's magnet programs.

II. METHODS AND SAMPLES

A. Evaluation of Cu–Nb–Sn Phase Equilibria

To investigate phase equilibria, binary Nb–Sn and ternary Nb–Cu–Sn samples were prepared using two techniques. Powder samples were prepared by mixing powders of the pure elements (≥99.8 % purity) with a pestle and mortar under an Ar atmosphere. These mixtures were pressed into pellets at 750 MPa and sealed under Ar in fused silica tubes. Isothermal heat treatments of 2 weeks at 400 °C and 500 °C were then applied, and the samples quenched in ice water.

Diffusion couples were prepared by magnetron sputtering of a 5 μm thick Sn layer for binary Nb–Sn samples, and one Cu and one Sn layer with a total thickness of 7 μm for ternary samples, on a ground Nb substate (99.9 % purity). These ternary physical vapor deposition (PVD) samples were prepared with different layer thickness ratios to achieve Cu:Sn atomic ratios of 0.35, 0.6 and 1.2. Following pre-annealing (for ternary compositions), 7-day isothermal heat treatments were applied to each sample at 220 °C, 300 °C, 400 °C and 500 °C.

The spatial distribution of phases was then investigated by scanning electron microscopy (SEM), and their compositions and lattice parameters were evaluated by energy-dispersive X-ray (EDX) spectroscopy and X-ray diffraction (XRD).

To investigate thermal decomposition of nausite, a powder sample with the composition 67 at% Sn, 25 at% Nb and 8 at% Cu was heat-treated under an Ar atmosphere for 2 weeks at 500 °C. In-situ X-ray diffraction was performed during heating over a 2θ range of 29.5° to 35° with Cu-Kα radiation to identify the phase transformations, and differential scanning calorimetry (DSC) was performed with a ramp rate of 10 K/min to more precisely determine the transition temperatures. Based on these studies, and others not reported here, the Cu–Nb–Sn ternary phase diagram has been re-evaluated using CALPHAD (Computer Coupling of Phase Diagrams and Thermochemistry) methods.

B. Phase Transformations in Internal Tin Wires

Six internal tin Nb_3Sn wires were selected for study, to allow a comparison between designs developed in the FCC conductor development program and commercial wires (Table I).

Distributed tin wire layouts of the type developed by JASTEC and KAT for the FCC conductor development program are represented by a 0.8 mm wire from JASTEC [7], [9]. The distributed barrier wire developed by TVEL is represented by a 1.0 mm sample from a recent R&D billet, similar to the type previously reported [9] but with small d_{eff}. Three variants of commercial RRP wire from Bruker OST were included in the study: one 0.85 mm diameter wire procured for the production of HL-LHC quadrupole (MQXF) magnets, and two types with diameters of 1.0 mm and 0.7 mm procured for CERN's high field magnet program. The four distributed barrier wires have similar sub-element sizes, but they differ in composition, overall wire layout and Cu/non-Cu ratio (Table I).

The heat treatment cycles recommended for these wires differ significantly (Fig. 1), but in all cases they include one or more low temperature steps at 210 °C and/or ~400 °C, and a reaction step at ~650 °C. To study phase transformation behavior during low temperature heat treatment steps, a set of samples of each wire type was cut, and each was encapsulated in a quartz tube under vacuum. Heat treatments were then performed on batches of samples at 210 °C, 370 °C, 400 °C and 450 °C; and an additional heat treatment at 400 °C was performed for samples first held for 48 h at 210 °C. In each case, samples were removed from the furnace at the start of the isothermal segment and at regular intervals thereafter — every 25 h up to 100 h for the 370 °C heat treatment, every 12.5 h up to 50 h for the 450 °C heat treatment, and every 12 h up to 48 h in all other cases — and quenched in water. The temperatures and intervals were chosen to cover the range used for standard heat treatments for the wires concerned (Fig. 1). The stages at which samples were quenched are shown in Fig. 2.

The samples were then mounted in conductive resin for examination in cross-section, and polished for electron microscopy. Backscattered electron images at 20 kV were obtained of the

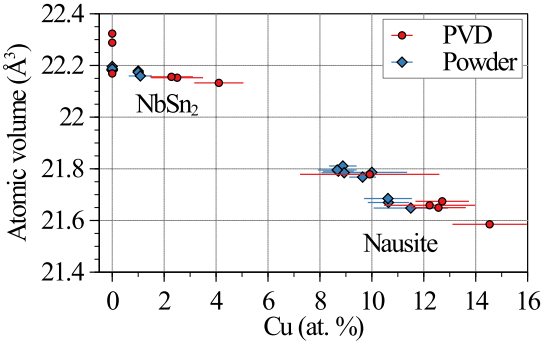

Fig. 3. Mean atomic volume as a function of copper molar fraction for PVD and powder samples containing nausite and/or $NbSn_2$ after isothermal annealing at 300–500 °C, as calculated from EDX and XRD analysis.

overall wire cross-section and of representative sub-elements at higher magnification. In selected cases, image analysis was performed on the sub-element micrographs, using previously reported Python scripts with the NumPy and SciPy libraries and toolkits [10], to calculate the area fraction of nausite and $NbSn_2$ relative to the sub-element area. The area fraction was averaged over 5–11 sub-elements in each case.

III. Evaluation of Cu–Nb–Sn Phase Equilibria

Heat treatment of diffusion couples prepared by PVD on a Nb substrate at 220 °C resulted only in the formation of Cu_6Sn_5 (η), but Nb participated in intermetallic phase formation at 300 °C and above. At 300 °C, nausite formed as plates with faceted interfaces to the surrounding melt, with the volume fraction of nausite increasing with the Sn concentration of the system. At 400 °C, a layer formed at the interface between η and Nb; and at 500 °C, above the decomposition temperature of η, $NbSn_2$ and Cu_3Sn (ε) formed. Nausite also formed on heat treatment of the powder mixtures at 400 °C and 500 °C: EDX analysis found that the Cu content decreased from 10–11.5 at% at 400 °C to 8.5–9.5 at% at 500 °C.

Many samples contained both $NbSn_2$ and nausite, which are very closely related, and indeed are challenging to distinguish. A detailed analysis of the structural relationships between the phases has recently been published [8]. Having resolved them in both PVD and powder samples, the composition and lattice parameters of each phase were obtained from EDX and XRD, and the mean atomic volume calculated. As shown in Fig. 3, both phases have a broad Cu composition range: up to ~4.5 at% solubility for $NbSn_2$, and a stability range of approximately 8–15 at% for nausite.

In-situ XRD of a nausite-containing powder sample was used to assess the phase transformations on decomposition of nausite (Fig. 4). Unfortunately the temperature was not accurately measured (due to the location of thermocouple), as is clear from the elevated temperature for tin melting; but it is nevertheless clear that at a higher temperature, the nausite reflections fade and those of $NbSn_2$ intensify simultaneously, indicating a decomposition of nausite $\rightarrow$ $NbSn_2$ + Sn(Cu). To determine the onset temperature of this process, DSC analysis was performed, as presented in Fig. 5. The melting of Sn and decomposition of η are clearly visible at the established temperatures. The peak with an onset at 586 °C is ascribed to the decomposition of nausite.

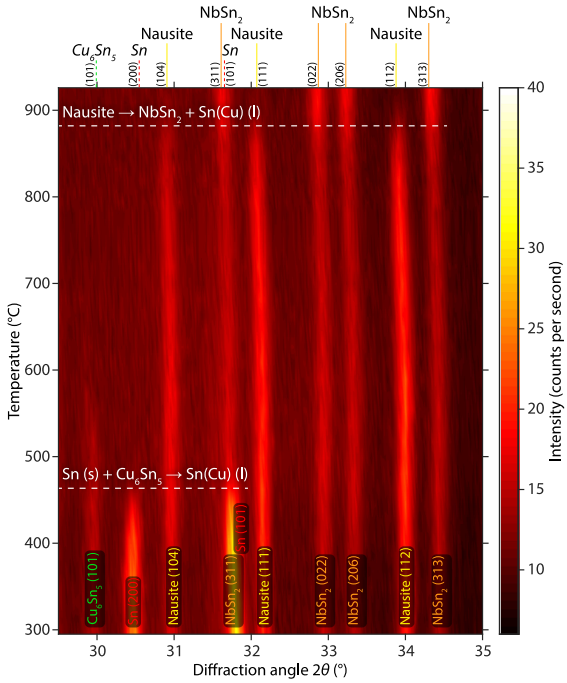

Fig. 4. High temperature X-ray diffraction data. The plotted temperature is that of the heating element, to which the thermocouple was attached: the sample temperature is significantly lower.

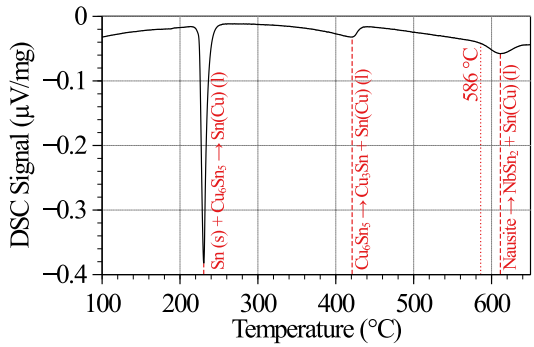

Fig. 5. Results of DSC analysis for a ternary Nb–Cu–Sn sample containing nausite. Peak positions are marked with red dashed lines, and the onset of nausite decomposition at ~586 °C is shown with a red dotted line.

For a Nb_3Sn wire heat treatment, this would occur during the ramp to the reaction step. These results, and others not reported here, are in use to develop a thermodynamic database for the Cu–Nb–Sn system to allow calculation of the ternary phase diagram using the CALPHAD method. Isothermal sections pertaining to the presently applied heat treatment temperatures have been calculated using a preliminary version of the database and are presented in Fig. 6.

IV. Analysis of Wire Micrographs After Low-Temperature Heat Treatment Steps

Micrographs of samples quenched from the step at 210 °C show, as expected, a shrinking tin core (bright white contrast), as outward diffusion of tin proceeds and Cu–Sn phases grow between the tin cores and the niobium filament regions. After

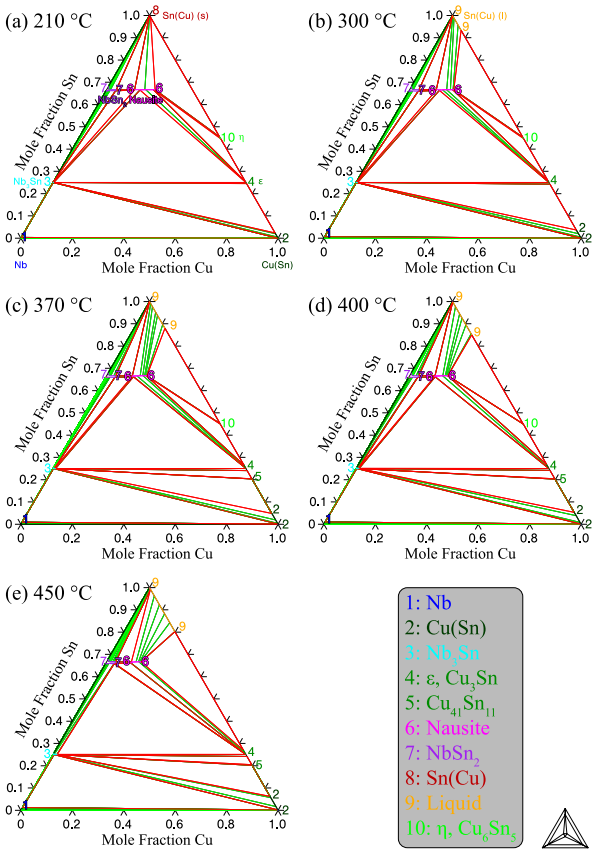

Fig. 6. Isothermal sections of the ternary Cu–Nb–Sn phase diagram at (a) 210 °C, (b) 300 °C, (c) 370 °C, (d) 400 °C, and (e) 450 °C.

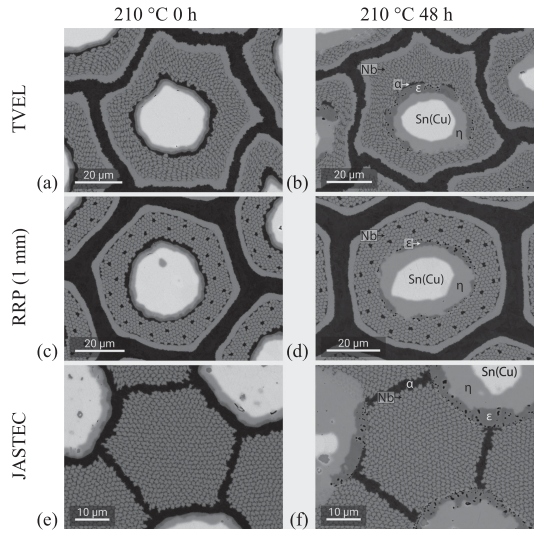

Fig. 7. Micrographs of wire samples quenched from the 210 °C isothermal heat treatment: the TVEL distributed barrier wire at (a) 0 h and (b) 48 h; the 1 mm diameter RRP wire at (c) 0 h and (d) 48 h; and the JASTEC distributed tin wire at (e) 0 h and (f) 48 h.

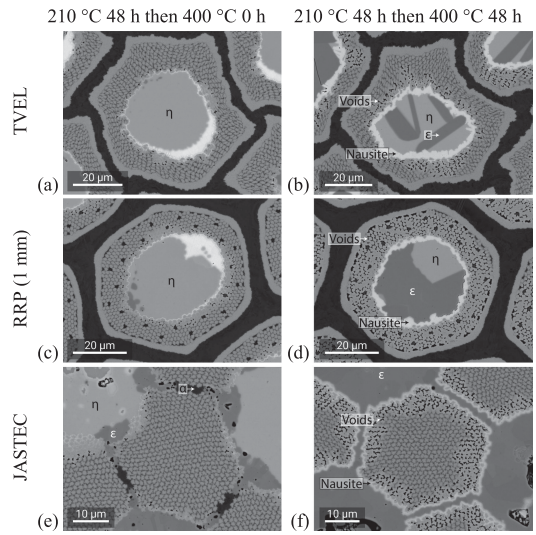

Fig. 8. Micrographs of wire samples quenched from the 400 °C isothermal heat treatment after 48 h at 210 °C: the TVEL distributed barrier wire at (a) 0 h and (b) 48 h; the 1 mm diameter RRP wire at (c) 0 h and (d) 48 h; and the JASTEC distributed tin wire at (e) 0 h and (f) 48 h.

48 h at 210 °C, this diffusion front has reached the niobium filaments for all five wire types, and Sn is separated from the Cu(Sn) surrounding the filaments by layers of Cu_6Sn_5 (η, light grey) and Cu_3Sn (ε, darker grey). When ε does extend to the Nb stack, voids are visible as dissolution of the interfilamentary Cu begins. This behavior is not markedly different between the wire types. Nb filaments adjacent to wider Cu channels or more distant from Sn sources remain in contact with almost pure Cu: e.g., for irregularly shaped sub-elements (TVEL, Fig. 7(b)), and where niobium modules are adjacent in distributed tin wires (JASTEC, Fig. 7(f)). Even in the absence of non-uniformity, there are cases for all wire types in which η extends into the interfilamentary copper past the ε ring (Fig. 7(b), (d) and (f)), as previously reported for RRP [2], [3].

At the end of the 210 °C step, some elemental Sn remained in all cases. By the end of the ramp to 400 °C (Fig. 8), some residual Sn(Cu) remained, but this was predominantly replaced by η, with a ring of nausite at the interface with the Nb filament region. In the distributed tin wire only, substantial pockets of ε have grown at the interface adjacent to the Cu channels between Nb modules (Fig. 8(e)), and some peripheral filaments in Nb modules remain in contact only with Cu(Sn). As the 400 °C step progresses, the nausite layer (bright white contrast) thickens, the core becomes increasingly Cu-rich as inward copper diffusion continues, and voids form progressively deeper into the interfilamentary region. Image analysis confirms this trend quantitatively: for both the TVEL wire and the RRP wires, the area fraction of nausite increases as a function of time (Fig. 10(a)).

For all three RRP wires, voids indicating Cu depletion of the interfilamentary region extend to the diffusion barrier after 48 h (e.g., Fig. 8(d)), and the majority of the core is converted to ε. For the TVEL wire, the Cu-depleted region is smaller and less uniform, and the core remains richer in Sn (Fig. 8(b)), due to slower diffusion through locally narrower Cu channels and/or the increased local thickness of the Nb filament region due to sub-element nonuniformity. This suggests that a longer step at ~400 °C would be advisable for the TVEL wires than the RRP wires presented here.

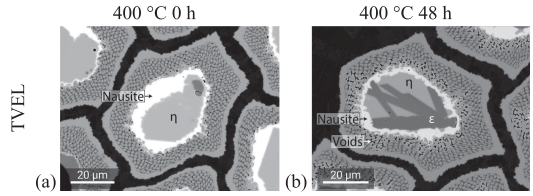

Fig. 9. Micrographs of the TVEL wire sample without a step at 210 °C quenched from (a) the start (0 h) and (b) the end (48 h) of the 400 °C step.

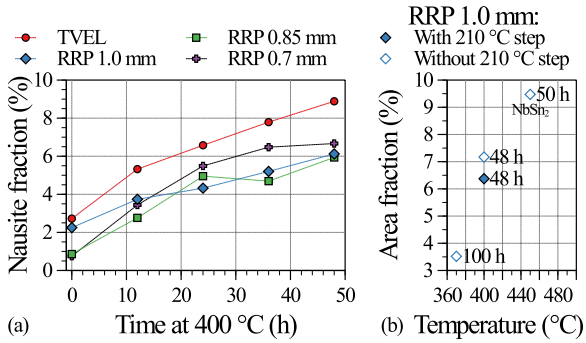

Fig. 10. Area fraction of nausite determined by image analysis for distributed barrier wires: (a) as a function of heat treatment duration at 400 °C, after a step at 210 °C, and (b) for the 1.0 mm diameter RRP wire at the end of the final isothermal step, as a function of temperature (with and without a prior step at 210 °C). Note that at 450 °C the main phase found in the high-Sn ring next to the Nb filaments is $NbSn_2$. Dashed lines are a guide to the eye only.

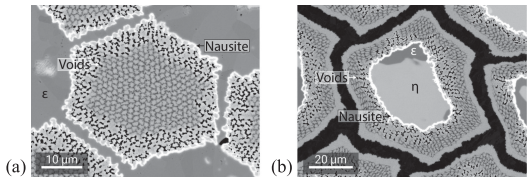

Fig. 11. Micrographs of wire samples quenched after a 100 h isothermal heat treatment at 370 °C: (a) JASTEC and (b) TVEL.

For the JASTEC wire, a much smaller portion of the interfilamentary region is Cu-depleted (Fig. 8(f)), but the remaining Sn content outside the filament region is also lower: almost no η remains, and voids occupy the original Sn cores. The same was also true after 100 h at 370 °C (Fig. 11(a)). This is due to the radius of the Nb module being larger than the thickness of the RRP filament region, and the additional accessible Cu outside the filament region. This suggests that nausite control is a lesser concern for distributed tin wires, and that shorter low-temperature steps are likely to be sufficient.

Comparing samples with and without an initial 210 °C step, a thicker layer of nausite has formed by the end of the ramp to 400 °C in the former case (Fig. 9); but after 48 h at 400 °C, there is almost no residual effect. This was previously reported for RRP wires [2], [3], and is confirmed here also for the TVEL and JASTEC layouts (Fig. 10(b)).

Increasing the intermediate heat treatment temperature from 370 to 400 °C markedly increases the area fraction of nausite, as shown in Fig. 10(b) for the 1.0 mm RRP wire, even considering that a longer duration (100 h) was applied at the lower temperature (370 °C). At 450 °C, the trend of a growing high-Sn ring next to the Nb filaments continues, but the phase present is primarily $NbSn_2$. It should be noted that after 100 h at 370 °C, the η fraction of the core remains much higher for both TVEL and RRP wires than after 48 h at 400 °C (Fig. 11(a)), suggesting that careful optimization of the temperature and duration is needed.

V. Conclusion

Phase equilibria studies of the Cu–Nb–Sn system have identified a broad Cu solubility range for both $NbSn_2$ and nausite, which are closely related phases. The Cu composition range of nausite decreases as the temperature increases, and the phase decomposes to $NbSn_2$ and Sn(Cu) at ~586 °C. A ternary phase diagram is in preparation, and isothermal sections in the low temperature range have been presented.

The behavior of both distributed tin (JASTEC) and distributed barrier (TVEL) wires during low temperature heat treatment steps is broadly similar to that of RRP wires; and different Sn stoichiometries have only a minor effect. This suggests that the heat treatment optimization principles proposed by Sanabria *et al.* remain applicable: the step at 210 °C is beneficial only for avoiding Sn bursts (especially in cables/coils [11]), and a relatively long step at a temperature below 400 °C is desirable to reduce the η content of Sn-rich regions without excessive nausite growth [2], [3].

There are, however, some differences between the wire types. For distributed tin wires, nausite control seems to be a lesser concern (as more Cu is accessible outside the filament region), and shorter low-temperature steps should be sufficient. It will be assessed in future studies whether the lower porosity of the interfilamentary region in this wire type is beneficial for compositional uniformity or Nb_3Sn growth kinetics.

For distributed barrier wires, the required heat treatment duration has been found to be sensitive to sub-element geometry due to its influence on diffusion kinetics. In all cases, however, 100 h at 370 °C was insufficient to achieve complete η to ε conversion. To realize the potential benefits of using a lower temperature than 400 °C, wire-specific optimization of the temperature and duration is therefore needed. An extension of this study to include Nb_3Sn formation and the resulting J_c and RRR performance is in progress.

Temperature ranges for nausite formation are broadly consistent between the diffusion couple and wire studies, but it should be noted that the wires studied are all Ti-doped: an extension of the phase equilibria studies to include dopants, alloying elements and internal oxidation is planned. Further study of the 400–450 °C temperature range is in progress.

Acknowledgment

The authors gratefully acknowledge the collaboration partners in the FCC conductor development program contributing to this work: TVEL and JASTEC, who provided the wire samples, and KEK, with whom wire development activities in Japan are jointly coordinated.

References

[1] A. Ballarino and L. Bottura, "Targets for R&D on Nb_3Sn conductor for high energy physics," *IEEE Trans. Appl. Supercond.*, vol. 25, no. 3, Jun. 2015, Art. no. 6000906.

[2] C. Sanabria, "A new understanding of the heat treatment of Nb_3Sn superconducting wires," Ph.D. dissertation, Florida State Univ., Gainesville, FL, USA, 2017. [Online]. Available: http://purl.flvc.org/fsu/fd/FSU_2017SP_Sanabria_fsu_0071E_13761

[3] C. Sanabria, M. Field, P. J. Lee, H. Miao, J. Parrell, and D. C. Larbalestier, "Controlling Cu–Sn mixing so as to enable higher critical current densities in RRP Nb_3Sn wires," *Supercond. Sci. Technol.*, vol. 31, Apr. 2018, Art. no. 064001.

[4] M. Naus, "Optimization of internal-Sn Nb_3Sn composites," Ph.D. dissertation, Univ. Wisconsin-Madison, Madison, WI, USA, 2002. [Online]. Available: https://fs.magnet.fsu.edu/∼lee/asc/pdf_papers/theses/mtn02phd.pdf

[5] S. Martin, A. Walnsch, G. Nolze, A. Leineweber, F. Léaux, and C. Scheuerlein, "The crystal structure of $(Nb_{0.75}Cu_{0.25})Sn_2$ in the Cu–Nb–Sn system," *Intermetallics*, vol. 80, Jan. 2017, pp. 16–21.

[6] J. P. Charlesworth, I. Macphail, and P. E. Madsen, "Experimental work on the niobium-tin constitution diagram and related studies," *J. Mater. Sci.*, vol. 5, no. 7, pp. 580–603, Jul. 1970.

[7] A. Ballarino *et al.*, "The CERN FCC conductor development program: A worldwide effort for the future generation of high-field magnets," *IEEE Trans. Appl. Supercond.*, vol. 29, no. 5, Aug. 2019, Art. no. 601709.

[8] J. Lachmann, N. Huber, and A. Leineweber, "Nausite and $NbSn_2$ – growth and distinction of structural related intermetallic phases in the Cu–Nb–Sn system," *Mater. Charact.*, vol. 168, Oct. 2020, Art. no. 110563.

[9] S. C. Hopkins, A. Baskys, B. Bordini, J. Fleiter, and A. Ballarino, "Design, performance and cabling analysis of Nb_3Sn wires for the FCC study," *J. Phys.: Conf. Ser.*, vol. 1559, 2020, Art. no. 012026.

[10] S. C. Hopkins, A. Baskys, A. Canós Valero, and A. Ballarino, "Quantitative analysis and optimization of Nb_3Sn wire designs toward future circular collider performance targets," *IEEE Trans. Appl. Supercond.*, vol. 29, no. 5, Aug. 2019, Art. no. 6001307.

[11] C. Sanabria, I. Pong, L. P. LaLonde, and S. Prestemon, "Further heat treatment optimizations for Nb_3Sn conductors: From wires to cables," *IEEE Trans. Appl. Supercond.*, vol. 29, no. 5, Aug. 2019, Art. no. 6001104.